J Ther Eng, Vol. 10, No. 6, pp. 1465−1479, November, 2024

Journal of Thermal Engineering
Web page info: https://jten.yildiz.edu.tr
DOI: 10.14744/thermal.0000888

Research Article

Numerical analysis of three-dimensional magnetohydrodynamics non-Newtonian free stream flow induced by permeable stretching surface

Khyati DANG[1], Vinita MAKKAR[1,*], Naresh SHARMA[1]

[1]*Department of Basic and Applied Sciences, School of Engineering and Sciences, GD Goenka University, Gurgaon, Haryana, 122103, India*

ARTICLE INFO

Article history
Received: 09 August 2023
Revised: 23 January 2024
Accepted: 24 January 2024

Keywords:
Buongiorno's Model; Casson Fluid; Chemical Reaction; Nanofluid; Shooting Method; Three-Dimensional Magnetohydrodynamics Flow

ABSTRACT

The modern research aims to explore the influence of free stream flow on the motion of MHD Non-Newtonian nanofluid through a permeable extending surface in a three-dimensional domain. The primary goal of this research is to examine the significance of distinct fluid parameters, including Casson fluid parameter β, free stream velocity parameter λ, Brownian motion parameter *Nb*, magnetic parameter *M*, Prandtl number *Pr*, thermophoresis parameter *Nt*, Lewis number *Le* on distribution of velocity, concentration of nanoparticle and temperature. When similarity variables are incorporated into the set of governing partial differential equations, the equations are modified into a set of ordinary differential equations. Runge–Kutta fourth order is employed with the help of shooting approach in order to achieve the computational approach of the model that has been reduced. Numerical values of physical characteristics, like that the Nusselt number, the Sherwood number, and skin friction, have been assessed contrary to numerous parameters and disclosed in tables for the subject of engineering. Results for distribution of temperature, velocity and concentration of nanoparticles are explored in detail, including their rate of convergence. The principal results of the research revealed that the influence of both Casson fluid and magnetic parameter on the distribution of velocity exhibits a pattern of decline. Additionally, the effects of Brownian motion parameter on temperature demonstrate a rising pattern, while its impact on concentration distribution shows a diminishing trend. The use of permeable materials has shown that the heat transport process along an expanding surface prevents thermal loss and promotes the cooling process, which is a significant outcome of the study. The findings of this research have numerous applications in biomedical engineering and are useful for the analysis of fluids that are not Newtonian under various conditions. The recent study in the three-dimensional extending region is important for the development of novel industrial processes involving nanoparticles and the idea of magnetohydrodynamics flow of non-Newtonian fluids in existence of free stream flow.

Cite this article as: Dang K, Makkar V, Sharma N. Numerical analysis of three-dimensional magnetohydrodynamics non-Newtonian free stream flow induced by permeable stretching surface. J Ther Eng 2024;10(6):1465−1479.

***Corresponding author.**
*E-mail address: vini252011makkar@gmail.com

This paper was recommended for publication in revised form by Editor-in-Chief Ahmet Selim Dalkılıç

INTRODUCTION

Nanofluid are assumed to be the next big thing in manufacture technology. Nanofluids are fast becoming the next big thing in manufacturing technology. Nanotechnology is being used to improve equipment and procedures in order to increase productivity. A primary focus of nano-science in the manufacturing industry is in the enhancement of catalytic mechanisms. The next generation of highly effective automobile radiators-heat exchangers are being investigated with the use of platinum-based nanomaterials. With the use of nanotechnology, the construction industry is able to provide various possibilities in terms of style, safety, cost, and efficiency involving Nano-impregnated metal, glass, concrete or other materials. As a result of their little size, nanoparticles possess extraordinary characteristics. Because of their high density, they are able to pack efficiently, which increases the material's strength. Furthermore, nanoparticles frequently exhibit changed viscosity, which has the effect of changing the behavior of fluids. Furthermore, because of their increased thermal conductivity, they are useful for increasing the properties of heat transmission in a variety of applications.

The features of the nanoparticles that are scattered inside nanofluids have a substantial impact on the general efficiency of the fluid, and the behavior of nanofluids is closely connected to these qualities through a complicated connection. These nanoparticle characteristics, which are governed by parameters like as size, shape, and chemical composition, have an enormous effect on the total efficiency of nanofluids. When it comes to assessing the collective impact that nanoparticles have on density, viscosity, and thermal conductivity, the volume fraction of nanoparticles, also known as the concentration of nanoparticles in the fluid, is an extremely important factor. In proportion to the rise in the volume percent, the effect of nanoparticles on these attributes also increases significantly. Therefore, in order to anticipate and optimize the thermophysical characteristics of nanofluids, it is necessary to have a full understanding of these nanoparticle features and to precisely quantify them. This will make it possible for more accurate evaluations of the heat and fluidic behaviours of nanofluids. Choi and Eastman [1] proposed the notion of nanofluids to optimize heat transfer in thermal systems. They empirically demonstrated that the incorporation of nanoparticles (defined as particles with dimensions lower than 100 nm) with the conventional liquids, including ethylene glycol mixtures, water, or oil, significantly enhances the fluids' thermal conductivity and heat transfer capabilities.

A nanofluid is the term used to describe the sustained suspension and uniform dispersion of nanoparticles that occur within the base fluid. As a result of their heat transfer characteristics, nanofluids have been implemented as working fluids in numerous energy-conserving industrial processes, technological device manufacturing to reduce costs, and advanced medical treatments that save lives. Many researchers and academics are interested in studying nanofluids in order to take advantage of their high heat transfer rate. While fluids are in general less proficient in transferring heat than solids, nevertheless, Xuan and Li [2] found, experimentally using the hot-wire approach, that ultrafine particle inclusion improves nanofluid thermal conductivity. Buongiorno [3] developed an organized procedure that increased the thermal energy transport mechanism through thermophoresis diffusion and Brownian motion.

Nanoscale heat and mass transport analysis requires understanding nanoparticle behaviour in nanofluids. Nanofluids are base fluids with nanoscale particles that have unique thermal and fluidic characteristics. These fluids' heat and mass transmission properties depend on their temperature, speed, and nanoparticle concentration. Nanofluids' heat transmission efficiency depends on nanoparticle clustering or dispersion and their interactions with the base fluid. To better understand nanofluid dynamics and optimize their use in heat management systems, researchers is needed evaluate these qualities, concentrating on particle behaviour at the Nanoscale. By utilizing the numerical simulations, Koopaee et al. [4] explored the steady-state convection that occurs naturally of a water-Al2O3 nanoliquid inside a cavity with a square shape subject to electric fields of varying slope angles. In their study, Reddy et al. [5] employed the finite element method to simulate the influence of a magnetohydrodynamic surface layer flow and exchange of heat of nanoliquid across a flexible shrinking sheet equipped with a heat sink or source and partition mass vacuum.

Jelodari and Nikseresht [6] studied the Lorentz force's three-dimensional effects on electromagnetic nanofluid heat exchange in a cubic chamber and the impact of a magnetic induced current. Kilic and Ali [7] conducted a numerical study employing nanofluids with three affecting jets to explore the amplification of thermal and the movement of fluid away from a heated region. Shah et al. [8] established the hybrid nanoparticle that includes an exchange of heat process and flow design as a result of the force field. They noticed that the appearance of Lorentz forces boosts conduction efficiency. Using the Optimal Homotopy Analysis method, Three-dimensional second-class nanofluid flow via an elongated surface has been analyzed by Ahmad et al. [9], including thermophoresis & Brownian motion. They found that when the value of the second-order parameter rises, temperature and nanoparticle concentration both diminish.

Acharya et al. [10] examined the flow and heat transfer behavior of nanofluids flow when exposed to radiative solar radiation. Entropy production and Condensation of an Al_2O_3-water nano liquid inside a crown space has been examined by Dogonchi et al. [11] considering the influences of infrared radiation, permeable materials, the shape of the curvy wall, and the location of the chamber. The hydro-magnetic movement of mixed nanoliquids via a

flexible curved surface has been examined through Waqas et al. [12]. Thermal radiation, as well as heat sinks and sources, are considered in the thermal integrity study of the flow. Using suction/injection and a source of heat, Abo-Dahab et al. [13] demonstrated the MHD Casson nanoliquid transport mechanism through a porous medium that is affected by a chemical process on a rapidly heated exponential surface. 3 D movement of an ethylene glycol-based titanium nanoliquid has been analyzed by Swain and Mahanthesh [14] to determine the impact of nanoparticle dispersion. Ho et al. [15] evaluated the heat-shielding capability of alumina/water flow of a nanofluid in a constant-heat-flux metal pipe. Ahmed et al. [16] studied electrolytic convective formations in a thin magnetized nanofluid layer under fields of electricity and magnets. Selim et al. [17] analyzed the impacts of outer magnetic fields on electromagnetic nanofluids. In order to improve the transfer of heat in the manufacturing industry, Ullah et al. [18] looked into how to accurately anticipate the thermodynamic characteristics of nanofluids using computational fluid dynamics (CFD) and machine learning.

A scientific investigation of the behavior of a fluid that conducts electricity in the presence of an electrical field is known as magnetohydrodynamics (MHD). Alfven [19] suggested the idea of MHD in 1942. The study of MHD has significant implications in the medical, industrial and other sciences. Gundagani [20] analyzed the impact of radiant heat on turbulent magnetohydrodynamic movement in the vicinity of a vertical porous plate subject to varying suction. The impact of mass and heat exchange on the radiation-driven motion of a vertically permeable sliding sheet has been examined by Reddy et al. [21]. The research conducted by Sivaiah et al. [22] on the unstable MHD mixed convective motion across a vertically oriented porous surface in the context of radiation. Gundagani et al. [23] investigated the influence of energy on the motion of a semi-infinite vertically permeable sheet immersed in a medium that is porous with liquid dissipation in an unstable MHD convective movement.

Due to the temperature dependent viscosity of heating radiation, Deepa and Murali [24] explored the impact of greater-order chemical responses and thermophoresis on the transfer of energy and mass of an unsteady MHD free convective circulation via infinitely inclined porous plate. Considering a magnetohydrodynamic boundary layer in three dimensions, Gupta et al. [25] studied the convective motion and thermal transmission of water-driven metal and nanoparticles of alumina. Umar et al. [26] evaluated the movement of an Eyring-Powell fluid in three dimensions along an extending sheet, including the impacts of action energy and velocity slip. The flow of MHD Jeffrey nanofluids in porous materials under the impact of nonlinear heat emission and production or consumption of heat has been investigated by Abdullah Mohamedet al. [27].

The impact of electromagnetic flux, thermophoresis velocity, chemical processes and heat generation/absorption along a surface that is porous on the motion of an MHD boundary layer liquid with an exponentially expanding sheet has been examined by Jabeen et al. [28]. With convection boundary conditions and an exponentially expanding inclined surface, Anantha Kumar et al. [29] analyzed the dynamics and energy transportation coefficient of a Casson liquid under the influence of an electric field. The idea of triple diffusive circulation influenced by a magnetic field and moving in a direction of a power law governed expanding sheet is scrutinized by Goyal et al. [30]. A Two-dimensional boundary layer Williamson nanofluid in MHD flow past a stretching sheet that is not linear has been explored by Ahmed et al. [31]. Micro-rotational flow of MHD Williamson fluid via non-Darcy permeable materials has been scrutinized by Mishra et al. [32].

The investigation of non-Newtonian fluids has numerous real-world uses in technology and other fields of study. Non-Newtonian fluid mechanics has many interesting and important uses in the fields of manufacturing, healthcare and the applied disciplines. Casson [33] developed the first version of the Casson liquid model in 1959 to represent the color oil interlude flow. Murali et al. [34] considered changing suction in their investigation of the influence of a chemical response on the movement of a non-Newtonian liquid across a vast vertical surface in an unstable magnetohydrodynamic scenario. Bilal et al. [35] inspected the consequences of heat fusion and creation on movement of a non-Newtonian liquid past a three-dimensional surface employing the RKF numeric scheme.

Babu et al. [36] explored the effects of heat exchange, transverse electrical field, hall electricity, and turbulent dissipation on the unstable MHD organic convective Couette movement of a sticky, electronically conducting, inflexible, Casson liquid through an infinite vertically prone surface inserted into a porous structure. Ganesh Kumar [37] analyzed the behavior of Casson nanofluids in 3D radiative non-linear flow over an exponential surface using the Roseland approximation. Using a spectrum relaxation approach, Ibrahim and Anbessa [38] examined the Hall effect as well as the ion effect in conjunction with slip circumstances in 3D flow of non-Newtonian nanofluids along an exponential surface. The roles of thermo-diffusion and chemical process has been reviewed by Rao et al. [39] in the context of MHD movement of non-Newtonian nanoliquid enhanced by extending surfaces. Khan et al. [40] examined electromagnetic Casson nanofluids thermal energy distributions across a stretching sheet. MHD movement of Casson liquid via elongated surfaces has been studied by Venkata Ramudu et al. [41] considering advective conditions, with the impacts of Soret & Dufour fluxes and gradients accounted for.

The term “free stream, or upstream velocity” refers to the speed at which a fluid is moving prior to coming into contact with an impediment or approaching an enclosed space. In many areas of engineering, obtaining a concept of outer velocity is vital. For example, in the field of aerodynamics, it

assists in the process of determining the forces that act on a spacecraft or aircraft moving through the air. It is absolutely necessary for the study of the behavior of fluids in rivers, tubes, or channels in the field of hydrodynamics. Due to the influence of convection and conduction of heat energy on the free stream velocity, the upstream velocity also serves a vital part in the analysis of exchange of the heat from or to a surface.

The consequence of slip flow along with the free stream velocity over an extending cylinder in a presence of a hydromagnetic nanofluid has been discussed by Vinita and Poply [42]. Renu et al. [43] evaluated the consequences of applied magnetic-induction and an oblique outer velocity via a stretching surface in a Casson fluid heated from within. Wang and Zhao [44] studied the oscillating free stream velocities that occur in digital simulations of a rotor airfoil's unsteady aerodynamic properties. Nanoliquid flow over an elongated sheet with exponential radiation, and including both stable and dynamic fluid properties were studied by Irfan et al. [45]. The magneto hydrodynamic (MHD) movement of a viscous non-compressible outer velocity fluid through a stretched cylinder has been explored by Poply et al. [46].

The velocity of stretching, external electric fields, and material properties all affect product quality. Product strength and homogeneity depend on stretching velocity during fabrication. Furthermore, external electric fields can affect particle or molecule orientation in materials, affecting mechanical qualities and performance. Wires, tetra packs, glass fibers, polymers, and plastics provide different physical qualities that affect the product. Wire tensile strength, flexibility, conductivity, and glass fiber clarity and durability impact the final result. In order to achieve the necessary quality and performance in textiles, packaging, or other industrial applications, it is crucial to have a thorough grasp of these factors and to control them precisely.

The present research has the novelty that it is a new version in the field of permeable extending surfaces where the numerical solutions are achieved by the Runge-Kutta Fehlberg 45 procedure together with shooting approach towards the MHD non-Newtonian fluid's flow with the involvement of free stream velocity. The effects of thermophoresis and Brownian motion are also explored. Many scientists took an interest in this model because of its features and potential uses. This model has various uses, including in power plants, refrigeration systems, medical science, the automotive sector, and more. To yet, no study has been conducted on this subject. Flow velocity, fluid temperature, and nanoparticle concentration all exhibit different behaviors as a consequence of a wide range of critical, important physical parameters, and this study provides a considerable analysis and discussions drawn from appropriate graphs and from numerical information presented in tables. The following section present the mathematical model and its explanations. The recommended numerical approach is then described, Generated results are then discussed including graphical representations and their physical interpretation, and finally the paper's conclusions are presented highlighting the most significant results obtained.

MATHEMATICAL FORMULATION

In modern study, three dimensional flows of non-Newtonian nanofluid with outer velocity in existence of magnetohydrodynamic flow encouraged by permeable expanding surface has been investigated. The flow diagram of the given problem is shown in Figure 1. In this case, the sheet is elongated across the *xy*- direction and fluid is arranged in the *z* direction. A fixed magnetic flux B_o acts as usual in the direction of motion along the sheet. This study involves Brownian motion and thermophoresis impacts by employing Buongiorno's model. We suppose that $u = U_w = ax$ *and* $v = V_w = by$ denote the sheet velocity in the *x* & *y*-axis appropriately, and the constants *a* and *b* are used. The governing equations of the model are shown as [3, 47, 48]

Equation of Continuity

$$\frac{\partial u}{\partial x}+\frac{\partial v}{\partial y}+\frac{\partial w}{\partial z}=0, \tag{1}$$

Equation of Momentum in *x* and *y* direction

$$u\frac{\partial u}{\partial x}+v\frac{\partial u}{\partial y}+w\frac{\partial u}{\partial z}=\nu\left(1+\frac{1}{\beta}\right)\frac{\partial^2 u}{\partial z^2}-\left[\frac{\sigma B_0^2}{\rho}+\frac{\nu}{k_1}\left(1+\frac{1}{\beta}\right)\right]u + U_\infty\frac{\sigma B_0^2}{\rho}+U_\infty\frac{\partial U_\infty}{\partial z}, \tag{2}$$

$$u\frac{\partial v}{\partial x}+v\frac{\partial v}{\partial y}+w\frac{\partial v}{\partial z}=\nu\left(1+\frac{1}{\beta}\right)\frac{\partial^2 v}{\partial z^2}-\left[\frac{\sigma B_0^2}{\rho}+\frac{\nu}{k_1}\left(1+\frac{1}{\beta}\right)\right]v + U_\infty\frac{\sigma B_0^2}{\rho}+U_\infty\frac{\partial U_\infty}{\partial z}, \tag{3}$$

Equation of Energy

$$u\frac{\partial T}{\partial x}+v\frac{\partial T}{\partial y}+w\frac{\partial T}{\partial z}=\frac{k}{(\rho C_p)_f}\frac{\partial^2 T}{\partial z^2}+\frac{(\rho C_p)_p}{(\rho C_p)_f}\left[\frac{D_T}{T_\infty}\left(\frac{\partial T}{\partial z}\right)^2+D_B\frac{\partial T}{\partial z}\frac{\partial C}{\partial z}\right], \tag{4}$$

Equation of Concentration

$$u\frac{\partial C}{\partial x}+v\frac{\partial C}{\partial y}+w\frac{\partial C}{\partial z}=\frac{D_T}{T_\infty}\frac{\partial^2 T}{\partial z^2}+D_B\frac{\partial^2 C}{\partial z^2}-Kr(C-C_\infty), \tag{5}$$

The various elements of velocity across the *x, y*, and *z* axes are indicated through *u, v*, and *w* in preceding equation. *C* denotes the fluid concentration, ρ stand for fluid density, *T* denotes the fluid temperature, ν stands for kinematic viscosity, k_1 denotes the permeability, *Kr* denotes the chemical reaction parameter, D_B designates the Brownian motion, D_T designates the coefficient of thermophoresis diffusion and c_p represents the specific heat capacity.

along with the boundary conditions:

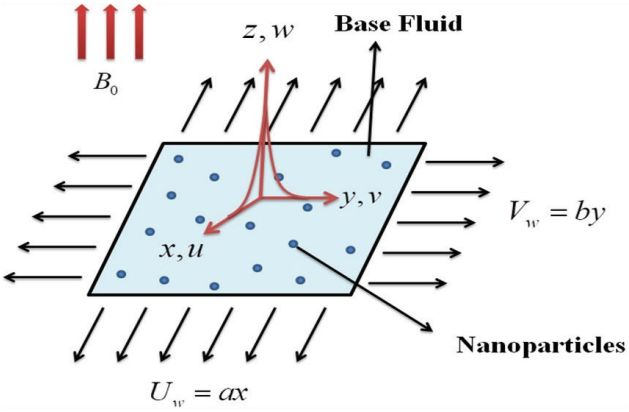

Figure 1. Physical diagram.

$$u = U_w = ax, \quad v = V_w = by \quad at \quad w = 0,$$
$$T = T_w, \quad C = C_w \quad at \quad z = 0$$
$$u \to 0, \quad v \to 0, \quad T \to T_\infty, \quad C \to C_\infty \quad as \quad z \to \infty \tag{6}$$

where T_∞ denotes the ambient temperature, T_w is the temperature at the surface, C_∞ stand for ambient concentration and C_w is the nanoparticle concentration at the surface, appropriately, where wall temperature is greater than ambient temperature.

Using Similarity variables [47]

$$\eta = \sqrt{\frac{a}{\nu}}z, \quad \theta = \frac{T - T_\infty}{T_w - T_\infty}, \quad \phi = \frac{C - C_\infty}{C_w - C_\infty}, \quad u = axf'(\eta),$$
$$v = byg'(\eta) \ and \ \ w = -\sqrt{a\nu[f(\eta) + cg(\eta)]}\,, \tag{7}$$

The radiative flux of heat q_r is calculated employing the Rosseland approximation, which is indicated by [49]

$$q^r = \frac{-4\,\sigma^*}{3k^*}\frac{\partial T^4}{\partial z}, \tag{8}$$

The abbreviation k^* signifies the coefficient of mean absorption, while σ* stands for the Stefan-Boltzmann constant. T^4 can be explained as a temperature-dependent linear function. Taylor series expansion of T^4 over T_∞, ignoring higher terms. The subsequent results are approximated as

$$T^4 \cong 4T_\infty^3 - 3T_\infty^4 \tag{9}$$

By using equations (8) and (9), we obtain the following form:

$$\frac{\partial q_r}{\partial z} = -\frac{16\sigma^* T_\infty^3}{3k^*}\frac{\partial^2 T}{\partial z^2}\,, \tag{10}$$

The incompressibility condition holds, hence eqs. (2)–(6) are transformed into eqs. (11) – (15)

$$\left(1+\tfrac{1}{\beta}\right)f''' - f'^2 + (f+cg)f'' - K_1\left(1+\tfrac{1}{\beta}\right)f' - M(f'-\lambda) + \lambda^2 = 0, \tag{11}$$

$$\left(1+\tfrac{1}{\beta}\right)g''' - cg'^2 + (f+cg)g'' - K_1\left(1+\tfrac{1}{\beta}\right)g' - M(g'-\lambda) + \lambda^2 = 0, \tag{12}$$

$$\Theta'' + Pr\left[(f+cg)\Theta' + Nb\Theta'\Phi' + Nt\Theta'^2\right], \tag{13}$$

$$\Phi'' + LePr(f+cg)\Phi' + \left(\frac{Nt}{Nb}\right)\Theta'' - Le\ PrCr\Phi = 0, \tag{14}$$

Reduced boundary conditions are:

$$f' = 1, \quad g' = 1, \quad \Theta(0) = 1, \quad \Phi(0) = 1,$$
$$f' \to \lambda, \quad g' \to 0, \quad \Theta \to 0, \quad \Phi \to 0, \tag{15}$$

Where fluid parameters are defined as follows:

$$M = \frac{\sigma B_0^2}{\rho a}, \quad c = \frac{b}{a}, \quad Cr = \frac{Kr}{a}, \quad Nt = \frac{\tau D_T(T_w - T_\infty)}{\nu T_\infty},$$
$$Nb = \frac{\tau D_B(C_w - C_\infty)}{\nu}, \ Le = \frac{\alpha}{D_B}, \ Pr = \frac{\nu\rho C_p}{k}, \ K = \frac{\nu}{ak_1} \tag{16}$$

Cf_x, Cf_y, Nu_x and Sh_x are all physical quantities established in terms of their non-dimensional counterparts.

$$Cf_x = \frac{\tau_{xz}}{\rho U_w^2}, Cf_y = \frac{\tau_{yz}}{\rho U_w^2}, \quad Nu_x = \frac{-x}{(T_w - T_\infty)}\left(\frac{\partial T}{\partial z}\right)|_{z=0}\,,$$
$$Sh_x = \frac{-x}{(C_w - C_\infty)}\left(\frac{\partial C}{\partial z}\right)|_{z=0} \tag{17}$$

Utilising the similarity variables (6) allows for the determination of the reduced Cf_x, Cf_y, Nu_x and Sh_x.

$$Cf_x\, Re_x^{1/2} = \left(1+\tfrac{1}{\beta}\right)f''(0), \quad Cf_y\, Re_x^{1/2} = \left(1+\tfrac{1}{\beta}\right)g''(0),$$
$$Nu_x\, Re_x^{-1/2} = -\Theta'(0), \ Sh_x\, Re_x^{-\frac{1}{2}} = -\Phi'(0), \tag{18}$$

Here Re_x is local Reynolds number.

Numerical Scheme

As a consequence of the substantially non-linear character of the differential equations (11)–(14), as well as the boundary equation (12), it is not possible to solve them analytically. The shooting algorithm shown in Figure 2 has been developed in MATLAB using the Runge-Kutta Fehlberg method and the ODE45 solver. When compared to other computational procedures, the shooting method's fifth-order truncation error is a substantial benefit. Moreover, the solution computing procedure is simplified in comparison to other numerical methods. MATLAB programming is used both to calculate graphical and tabular representations of the results. First, Equations (11)–(14) are modified into first-order differential equations. In order to accomplish this, transformed ODEs are re-organized into the following arrangement:

$$f''' = \frac{1}{\left(1+\frac{1}{\beta}\right)}\left[f'^2 - (f+cg)f'' + k_1\left(1+\frac{1}{\beta}\right)f' + M(f'-\lambda) - \lambda^2\right], \tag{19}$$

$$g''' = \frac{1}{\left(1+\frac{1}{\beta}\right)}\left[cg'^2 - (f+cg)g'' + k_1\left(1+\frac{1}{\beta}\right)g' + M(g'-\lambda) - \lambda^2\right], \tag{20}$$

$$\Theta'' = -Pr\left[(f + cg)\Theta' + Nb\Theta'\Phi' + Nt\Theta'^2\right], \quad (21)$$

$$\Phi'' = -\left[LePr(f + cg)\Phi' + \left(\frac{Nt}{Nb}\right)\Theta'' - LePrCr\Phi\right], \quad (22)$$

Now, a new set of components is defined to convert the previously mentioned eqs. into first-order (ordinary differential equations) ODEs.

$$\begin{aligned} f &= \varsigma_1, & f' &= \varsigma_2, & f'' &= \varsigma_3, & f''' &= \varsigma_3' \\ g &= \varsigma_4, & g' &= \varsigma_5, & g'' &= \varsigma_6, & g''' &= \varsigma_6' \\ \Theta &= \varsigma_7, & \Theta' &= \varsigma_8, & \Theta'' &= \varsigma_8' \\ \Phi &= \varsigma_9, & \Phi' &= \varsigma_{10}, & \Phi'' &= \varsigma_{10}' \end{aligned} \quad (23)$$

The system of differential equations acquired by substituting Equation (19) into Equations (15) to (18) is as follows:

$$\varsigma_1' = \varsigma_2 \quad (24)$$

$$\varsigma_2' = \varsigma_3 \quad (25)$$

$$\varsigma_3' = \frac{1}{\left(1 + \frac{1}{\beta}\right)}\left[\varsigma_2^2 - (\varsigma_1 + c\varsigma_4)\varsigma_3 + k_1\left(1 + \frac{1}{\beta}\right)\varsigma_2 + M(\varsigma_2 - \lambda) - \lambda^2\right], \quad (26)$$

$$\varsigma_4' = \varsigma_5 \quad (27)$$

$$\varsigma_5' = \varsigma_6 \quad (28)$$

$$\varsigma_6' = \frac{1}{\left(1+\frac{1}{\beta}\right)}\left[c\varsigma_5^2 - (\varsigma_1 + c\varsigma_4)\varsigma_6 + k_1\left(1 + \frac{1}{\beta}\right)\varsigma_5 + M(\varsigma_5 - \lambda) - \lambda^2\right], \quad (29)$$

$$\varsigma_7' = \varsigma_8 \quad (30)$$

$$\varsigma_8' = -Pr[(\varsigma_1 + c\varsigma_4)\varsigma_8 + Nb\varsigma_8\varsigma_{10} + Nt\varsigma_8^2], \quad (31)$$

$$\varsigma_9' = \varsigma_{10} \quad (32)$$

$$\varsigma_{10}' = -LePr\left[(\varsigma_1 + c\varsigma_4)\varsigma_{10} - \left(\frac{Nt}{Nb}\right)\varsigma_8' + LePrCr\varsigma_9\right], \quad (33)$$

The following are the final boundary conditions:

$$\begin{aligned} &\varsigma_2(0) = 1,\ \varsigma_5(0) = 1,\ \varsigma_7(0) = 1,\ \varsigma_9(0) = 1, \\ &\varsigma_2(\eta) \to \lambda,\ \varsigma_5(\eta) \to 0,\ \varsigma_7(\eta) \to 0,\ \varsigma_9(\eta) \to 0\ as\ \eta \to \infty \end{aligned} \quad (34)$$

We have used the shooting approach to obtain approximations of the aforementioned initial unknowns and utilised them in the solution, based on the previously

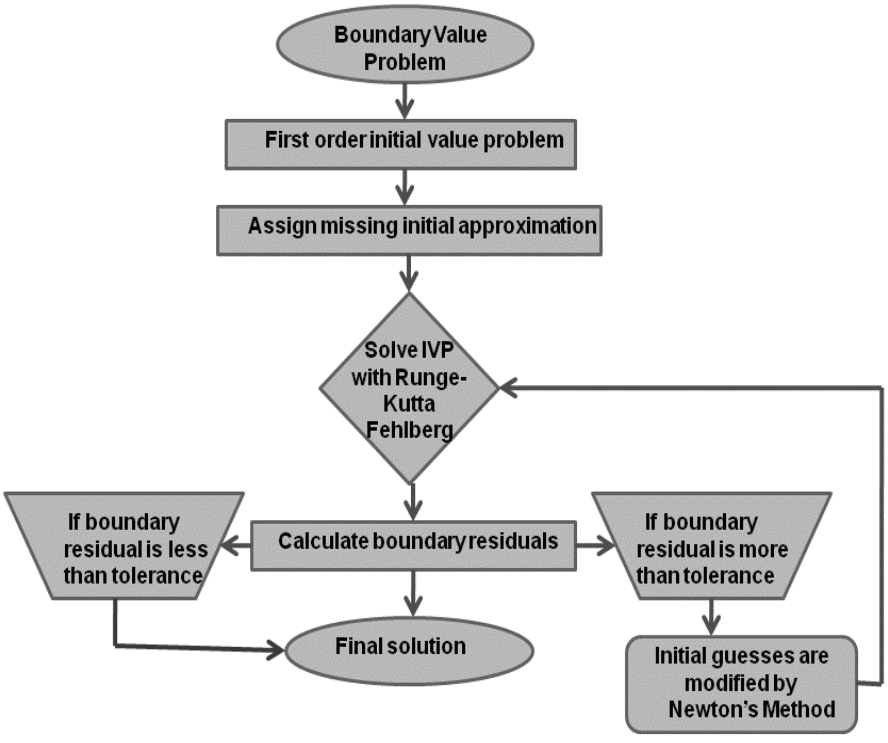

Figure 2. Schematic depiction of the shooting process.

mentioned assumption. Linear interpolation is employed to determine the unknown value by incorporating an initial grid with unequal spaces into the boundary condition. Space lengths are relatively short when closest to the surface and gradually increase in size as one moves away from it. The convergence criteria tolerance (F_i = 1,2,3) is equal to $|F_i| = 10^{-6}$, with

$$F_1 = y_2(\infty, A_1) - f'(\infty),\ F_2 = y_3(\infty, A_2) - g'(\infty),$$
$$F_3 = y_5(\infty, A_3) - \Theta(\infty),\quad F_4 = y_7(\infty, A_4) - \Phi(\infty). \quad (35)$$

RESULTS AND DISCUSSION

This section's objective is to conduct an investigation into the impact that a variety of physical parameters have on physical quantities like temperature, dimensionless velocities, and nanoparticle concentration. The Runge-Kutta Fehlberg method, implemented here with MATLAB code and the ODE45 solver, has been used to resolve a structure of (differential equations) DEs. Results are contrasted with the works of Abolbashari et al. [50], Reddy Gorla and Sidawi [51] and Wang [52] as shown in Table 1 which lists the residual errors over a range of Pr values using fixed values of k_1 = 0.1, M = 1.5, Nb = 0.1, Le = 2, Nt = 0.5, Pr = 0.73, Cr = 0.5, Tables 2-4 display the character of (f"(0) and g"(0)), ($-\Theta'(0)$), ($-\Phi'(0)$) in a serial manner for modification in several fluid parameters.

In Figure 3, the effect of the velocity distribution on the permeability parameter k_1, free stream velocity parameter λ, Casson fluid parameter β and the magnetic parameter M is illustrated. The changes in the velocity distribution caused

Table 1. Discussion for $-\Theta'(0)$ with variation in Pr: a comparison

Pr	Abolbashari et al. [50]	Residual Error	Reddy Gorla and Sidawi [51]	Residual Error	Wang [52]	Residual Error	Present Result
0.7	0.5349	-0.00055	0.4539	-0.00055	0.4539	-0.00055	0.45445
2	0.9114	-0.00055	0.9114	-0.00055	0.9114	-0.00055	0.91135
7	1.8905	0.00000	1.8954	-0.00490	1.8954	-0.00490	1.89540
20	-	-	3.3539	0.00000	3.3539	0.00000	3.35390
70	-	-	6.4622	0.00001	6.4622	0.00001	6.46219

Table 2. The values k_1, λ, β and M together with the skin friction coefficients (f"(0) and (g"(0)

k_1	λ	β	M	(f"(0)	(g"(0)
0.1	0.1	0.1	1.5	-0.594010981603266	-0.645430358456673
0.2	-	-	-	-0.674332887514870	-0.719025632569359
0.3	-	-	-	-0.745560602428051	-0.785740332795323
0.4	-	-	-	-0.810288155742902	-0.847172447339569
0.5	-	-	-	-0.870072169835853	-0.904403135899120
0.1	0.1	-	-	-0.594010981603266	-0.645430358456673
-	0.2	-	-	-0.559830094235799	-0.616807056011384
-	0.3	-	-	-0.522276043468497	-0.585620324816160
-	0.4	-	-	-0.481446249367520	-0.551974622659931
-	0.5	-	-	-0.437440336545568	-0.515964307344557
-	0.1	0.1	-	-0.594010981603266	-0.645430358456673
-	-	0.3	-	-0.860081087972717	-0.947343170552575
-	-	0.5	-	-1.011278626988158	-1.117734122793747
-	-	0.7	-	-1.113055895190225	-1.232193638403197
-	-	0.9	-	-1.187235866743442	-1.315531212594792
-	-	0.1	1	-0.562905153860447	-0.617733332665949
-	-	-	2	-0.623673507669170	-0.672298883035866
-	-	-	3	-0.679346322464002	-0.723618878950130
-	-	-	4	-0.730988027187760	-0.771976510832896
-	-	-	5	-0.779340147975374	-0.817724934548010

by the permeability parameter k_1 are shown in Figure 3(a), (b).This graph demonstrates that the distribution of velocities is increasing due to the presence of a greater quantity of nanofluid further away from the boundary, which in turn decreases the width of boundary region. Figure 3(c),(d) demonstrates the effects of the free stream velocity parameter λ on the distribution of velocity. The distribution of velocity and λ were shown to be directly proportional to one another. Therefore, a boost in the velocity of free stream will lead to enhance in the distribution of velocity. Figure 3(e) shows the effects of the Casson fluid parameter, which is a non-Newtonian parameter on the distribution of velocity. The velocity profile is shown to decrease with high values of the Casson parameter. This trend occurs because decreasing the yield stress, which is achieved by improving the fluid viscosity, is a result of raising the values of the Casson parameter. Hence, the thickness of the momentum boundary layer decreases. The influence of the magnetic parameter M on the velocity distribution as seen in Figure 3(f). Fluid velocity is reduced by Lorentz forces (The Lorentz force, a fundamental concept in electromagnetism, refers to the force encountered by a particle that is charged as it traverses an electromagnetic field.) as M increases, resulting in a decreasing velocity. The width of the surface layer and magnitude of the velocity distribution decrease in these directions.

As shown in Figure 4(a)-(d), the effect of the temperature distribution on fluid parameters like Brownian motion parameter *Nb*, thermophoresis parameter *Nt*, Lewis number *Le* and the Prandtl number *Pr* are all demonstrated. Figure 4(a) represents the effects of the Brownian motion parameter *Nb* on the temperature profiles. The collision between atoms or molecules of the fluid particles will generate a random movement known as Brownian motion of suspended particles, hence increasing the breadth of the boundary layer. An increase in the Brownian motion parameter *Nb* causes the fluid temperature to rise. The influence of the thermophoresis parameter *Nt* on the temperature profiles as seen in Figure 4(b). With an increase in *Nt*, the flow temperature rises. And the reason behind this is because the surface moves very quickly due to the force created by the temperature variation, which in turn causes the temperature to rise. Figure 4(c) reflects variation of temperature distribution against Lewis number

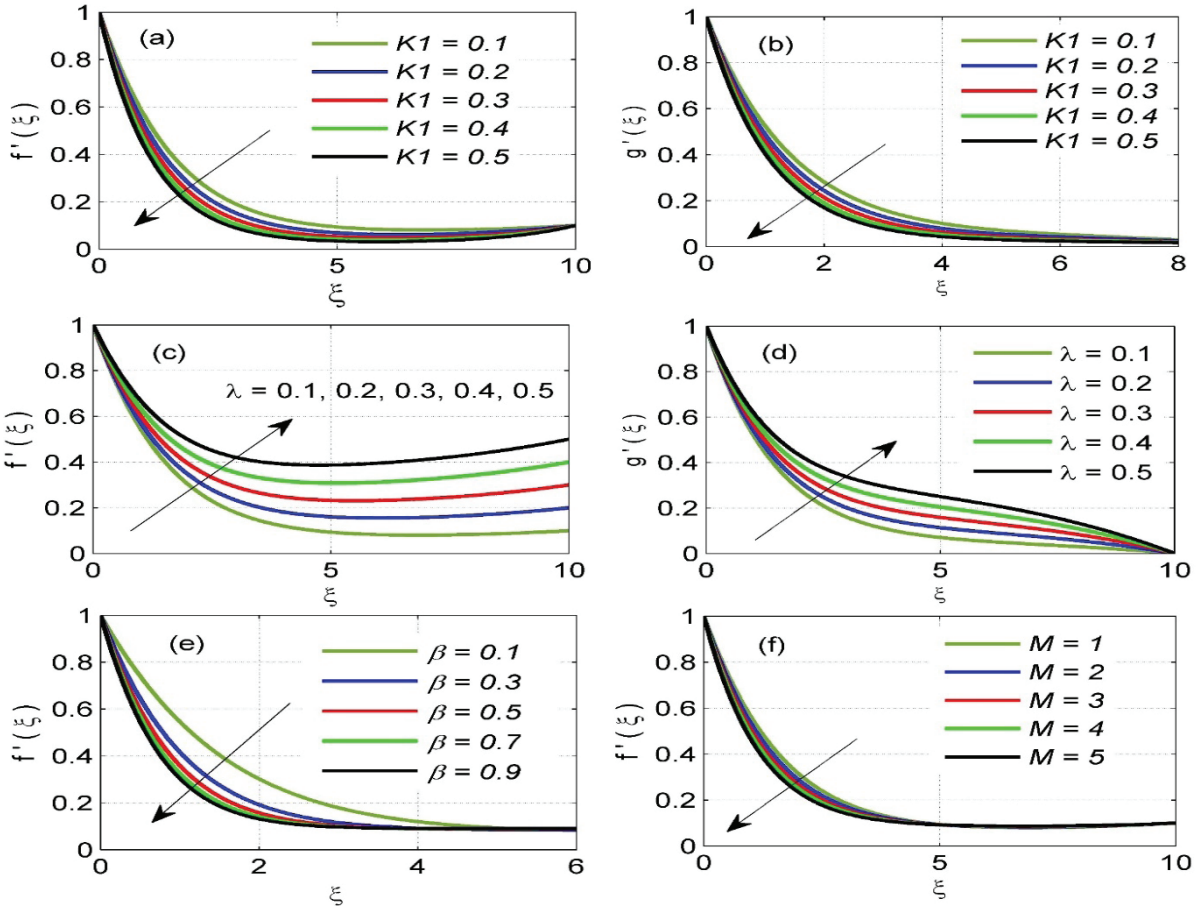

Figure 3. Velocity distribution ($f'(\xi)$) and $g'(\xi)$) for values of (a and b) k_1 ($0.1 \le k_1 \le 0.5$) and (c and d) λ ($0.1 \le \lambda \le 0.5$), Velocity distribution $f'(\xi)$ for values of (e) β ($0.1 \le \beta \le 0.9$) and (f) M ($1 \le M \le 5$).

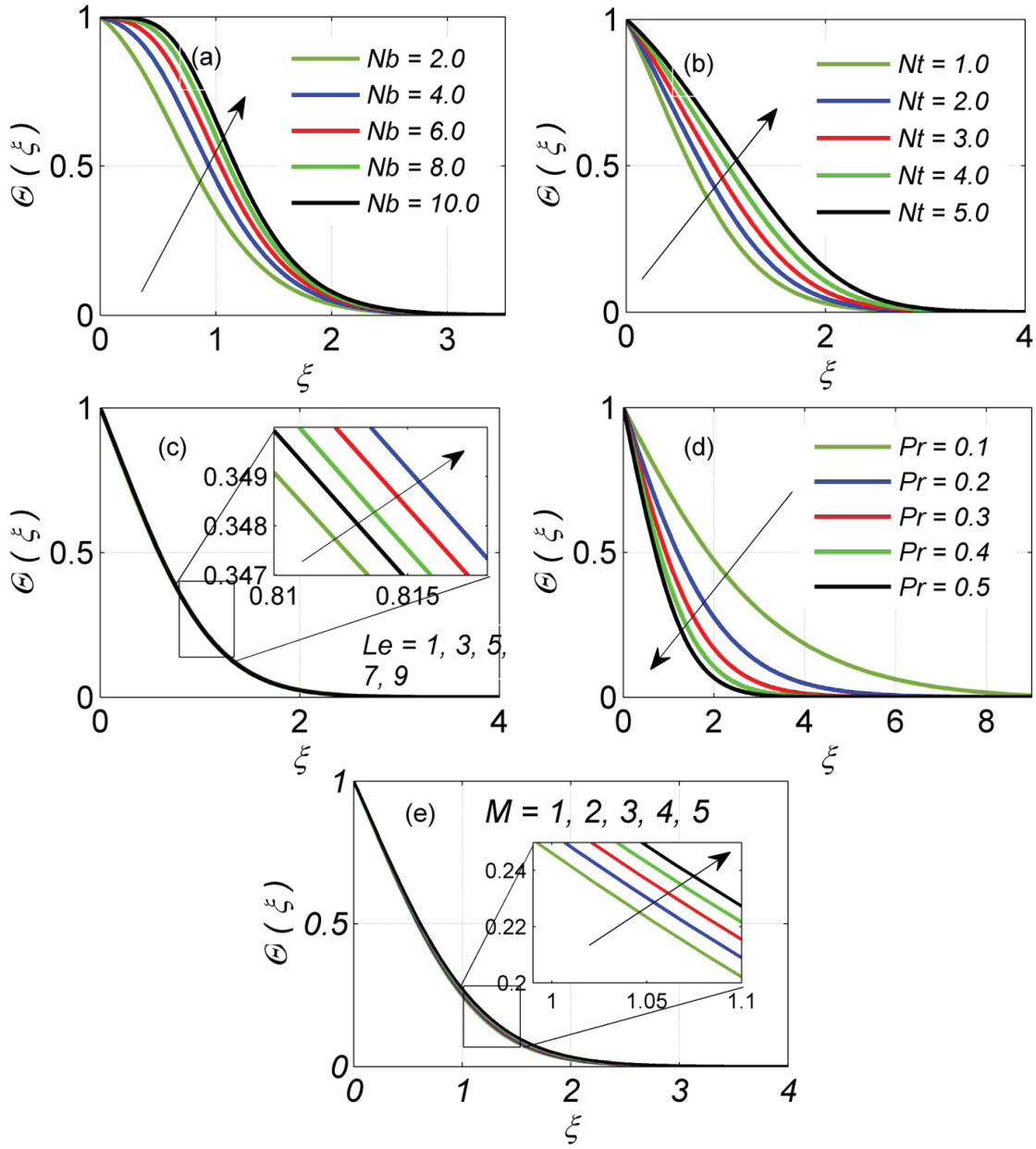

Figure 4. Temperature distribution ($\Theta(\xi)$) for various values of (a) Nb ($2.0 \le Nb \le 10.0$), (b) Nt ($1.0 \le Nt \le 5.0$), (c) Le ($1 \le Le \le 9$), (d) Pr ($0.1 \le Pr \le 0.5$), (e) M ($1 \le M \le 5$).

Le. This figure clearly indicates that the dimensionless temperature falls slightly as *Le* moves upward and rises slightly as *Le* moves downward. In the boundary layer system, the proportion of the thermal dissipation rate to the species dissipation rate is conveyed by the coefficient *Le*. The boost in the *Le* values will conclude to a drop in the width of the thermal surface region, which will be followed by a drop in temperature. Figure 4(d) examines the changes in temperature over various Prandtl number *Pr* values. Improving the *Pr* results in a decline in temperature. A fluid's thermal diffusivity has a significant impact on its Prandtl number. With a higher Prandtl number, thermal diffusivity is reduced. A decrease in temperature is caused by this reduced thermal diffusivity. As the magnetic parameter rises, the temperature profiles grow, as seen in Figure 4(e). The temperature in the boundary layer would rise because the size of the velocity patterns would decrease as the magnetic parameter increased.

The impact of the concentration profile on various fluid parameters, including the Brownian motion parameter Nb, thermophoresis parameter *Nt*, Lewis number *Le*, chemical reaction parameter *Cr*, is illustrated in Figure 5(a)-(d). The effect of the Brownian motion parameter *Nb* on the Concentration profile is seen in Figure 5(a). As the

Table 3. The values *Nb, Nt, Le* and *Pr* together with the local Nusselt number ($-\Theta'(0)$)

Nb	*Nt*	*Le*	*Pr*	$-\Theta'(0)$
2	0.5	2	0.73	0.323062481691837
4	-	-	-	0.100659229536828
6	-	-	-	0.028742985820990
8	-	-	-	0.007779602053068
10	-	-	-	0.002036206019164
0.1	1	-	-	0.750742118652069
-	2	-	-	0.576209359951660
-	3	-	-	0.451851001121734
-	4	-	-	0.362326329506975
-	5	-	-	0.296937252455790
-	0.5	1	-	0.886330182247955
-	-	3	-	0.852391891594155
-	-	5	-	0.841615791907446
-	-	7	-	0.836070394332742
-	-	9	-	0.832622368163601
-	-	2	0.1	0.300315338986676
-	-	-	0.2	0.458042124653497
-	-	-	0.3	0.573770611175197
-	-	-	0.4	0.664268285465217
-	-	-	0.5	0.737691424763612

Table 4. The values *Nb, Nt, Le* and *Cr* together with the local Sherwood number ($-\Phi'(0)$)

Nb	*Nt*	*Le*	*Cr*	$-\Phi'(0)$
0.01	0.5	0.1	0.5	-14.343169560156705
0.02	-	-	-	-6.216977365044295
0.03	-	-	-	-3.508488203892950
0.04	-	-	-	-2.154424457447120
0.05	-	-	-	-1.342130555309154
0.1	1	-	-	-0.423517834966708
-	2	-	-	-0.420329708948165
-	3	-	-	0.534443857313025
-	4	-	-	1.799048327053634
-	5	-	-	3.067283473043958
-	0.5	1	-	-0.791825773681388
-	-	3	-	0.972853775985054
-	-	5	-	1.936461680609818
-	-	7	-	2.645897198200492
-	-	9	-	3.225253820113944
-	-	0.1	1.0	0.718975498071542
-	-	-	1.5	1.087279910633945
-	-	-	2.0	1.404400008890760
-	-	-	2.5	1.682584373790211
-	-	-	3.0	1.930407901990225

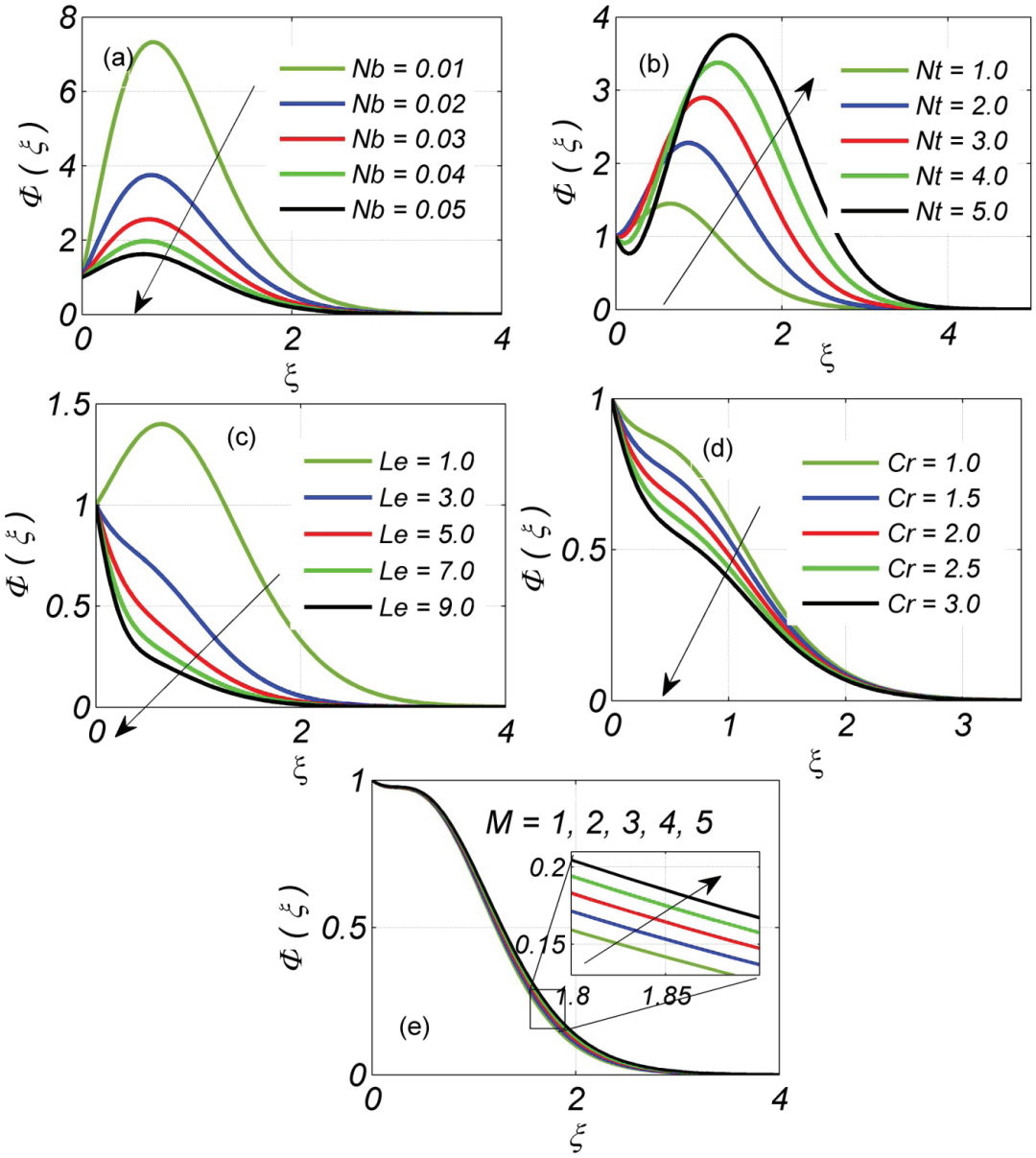

Figure 5. Concentration distribution ($\Phi(\xi)$) for various values of (a) *Nb* ($0.01 \le Nb \le 0.05$), (b) *Nt* ($1.0 \le Nt \le 5.0$), (c) *Le* ($1.0 \le Le \le 9.0$), (d) *Cr* ($1.0 \le Cr \le 3.0$), (e) *M* ($1 \le M \le 5$).

Brownian motion factor *Nb* grows, the molecules of the fluid move at random, leading to a fall in concentration and a rise in the rate of fluid conversion. Figure 5(b) depicts the relationship between nanoparticle concentration and the thermophoresis parameter. The concentration of nanoparticles grows as the thermophoresis parameter rises, as seen in the graph. In the occurrence of thermophoresis, the force exerted by one particle on other causes the other particles to shift from a hotter to a colder zone, which in turn causes the fluid to move from a hotter to a colder region, increasing the concentration of nanoparticles.

Figure 5(c) manifests the impact of Lewis number *Le* on nanoparticle concentration. As can be seen in Figure 5(c), as *Le* increases, concentration values decrease, effectively slowing the diffusion of nanoparticle species. Over a boost in the Lewis number, will occur a significantly bigger reduction in width of the concentration surface region than there will be in width of the warmth surface region. Figure 5(d) reflects the variation for nanoparticle concentration against the chemical reaction parameter *Cr*. As the chemical reaction parameter goes up, the distribution of concentration drops as is shown by 5(d). Figure 5(e) shows that the fluid's concentration profile, which is affected by the temperature gradient intrinsic in its viscosity, grows significantly as the magnetic parameter rises. Through contour plots, Figure 6(a)-(d) illustrates the effect of the skin friction coefficient on *Cr & Nt, Le & Nt,*

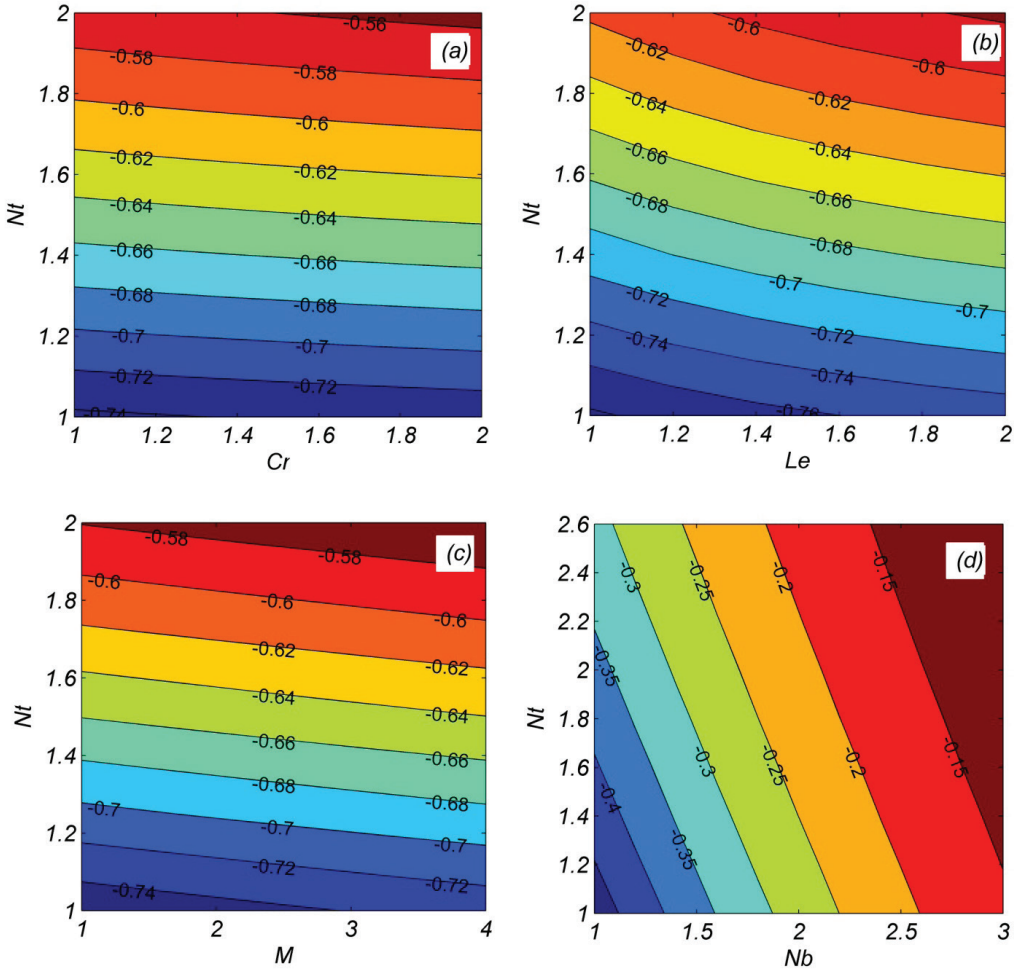

Figure 6. Skin friction coefficient against (a) *Cr* & *Nt,* (b) *Le* & *Nt,* (c) *M* & *Nt* and (d) *Nb* & *Nt*.

M & Nt and *Nb & Nt*, respectively. It can be shown from the contour plot in Figure 6(a) that skin friction increases when both the chemical reaction parameter $Cr(1 \leq Cr \leq 2)$ and the thermophoresis parameter Nt $(1 \leq Nt \leq 2)$ increase. Like Figure 6(a), Figure 6(b), Figure 6(c), and Figure 6(d) display the identical effect. The contour plots of skin friction reveal that, as shown in Figure 6(b), Figure 6(c) and Figure 6(d), skin friction grows with increasing $Le\ (1 \leq Le \leq 2)$ & $Nt\ (1 \leq Nt \leq 2)$, $M\ (1 \leq M \leq 4)$ & $Nt\ (1 \leq c \leq 2)$ and $Nb\ (1 \leq Nb \leq 3)$ & $Nt\ (1 \leq Nt \leq 2.6)$, respectively.

CONCLUSION

The current investigation looks at how MHD non-Newtonian nanofluids flowing through a porous material are affected by the presence of free stream flow. Our final results, which were calculated using the ODE45 solver in MATLAB, are contrasted with the results obtained by Abolbashari et al. [50] and Reddy Gorla and Sidawi [51] for to highlight the study's limitations. The results were concluded by comparing them to previous efforts and finding remarkable agreement. In addition to MHD, the present research highlights the importance of the exponential extending component and outer velocity on distribution of dimensionless temperature, velocity and nanoparticles concentration of flow, exchange of heat and mass of elastic fluid. The most important conclusions from this investigation are:

- As k_1 and β improves, the distribution of velocity reduces. In addition, the Lorentz drag force created by the presence of magnetism drops velocity when *M* is raised.
- A modification in the *Nb* and *Nt* improves the distribution of temperature. However, the temperature declines when the Prandtl number rises.
- The nanoparticle concentration goes down when *Cr* and *Le* increase, but it goes up when *Nt* is raised.
- In nanotechnology, the superior thermal conductivity of nanofluids makes them more valuable. Nanofluids are a type of fluid utilised in the field of nanotechnology as a coolant. The present findings may find greater application in nanotechnology.

- Since current research is more applicable to engineering systems, this article will be more relevant in the future.

The current study's findings have many real-world applications, including the insulation of wires, the production of tetra packs and fibres of glass, the refining of polymers and the creation of plastics as well as rubber sheets, and so on. The velocity of stretching, an external electric field, and the physical characteristics of the material all play a role in the final product's quality.

NOMENCLATURE

x, y, z	Cartesian coordinates
a,b	Positive constants
u, v, w	Components of velocity in the x, y, and z axes
T	Fluid temperature, K
T_w	Surface temperature
T_∞	Ambient temperature, K
M	Magnetic field parameter
Cr	Dimensionless chemical reaction parameter
C	Concentration of fluid, Kgm^{-3}
U_w, V_w	Velocities of the stretching sheet, $m^2\ s^{-1}$
C_w	Surface concentration, Kgm^{-3}
Nb	Brownian motion parameter, $m^2\ s^{-1}$
C_∞	Ambient concentration, Kgm^{-3}
$(\rho C)_p$	Effective heat capacity of a nanoparticle
D_B	Brownian diffusion coefficient
Pr	Prandtl number
B_0	Constant magnetic field
Nt	Thermophoresis parameter
C_{fx}	Skin friction coefficient in x−direction
D_T	Thermophoresis diffusion coefficient, $m^2\ s^{-1}$
$(\rho C)_f$	Heat capacity of the fluid $\tau = (\rho C)_p/(\rho C)_f$
f, g	Dimensionless stream functions
C_{fy}	Skin friction coefficient in y−direction
Nu_x	Local nusselt number
Sh_x	Local sherwood number
k_1	permeability parameter
Re_x	Local reynolds number
Kr	chemical reaction parameter

Greek symbols

υ	Kinematic viscosity of the fluid, $m^2\ s^{-1}$
Θ	Non−dimensional concentration
σ	Electrical conductivity
η	Similarity variable
β	Casson fluid parameter
ρ	Density of fluid, Kgm^{-3}
Φ	Non-dimensional temperature

Subscripts

f	Fluid
∞	Ambient condition
w	Wall
p	Particle

Subscripts

' Prime indicates a derivative with respect to η

AUTHORSHIP CONTRIBUTIONS

Authors equally contributed to this work.

DATA AVAILABILITY STATEMENT

The authors confirm that the data that supports the findings of this study are available within the article. raw data that support the finding of this study are available from the corresponding author, upon reasonable request.

CONFLICT OF INTEREST

The author declared no potential conflicts of interest with respect to the research, authorship, and/or publication of this article.

ETHICS

There are no ethical issues with the publication of this manuscript.

REFERENCES

[1] Choi SU, Eastman JA. Enhancing Thermal Conductivity of Fluids with Nanoparticles (No. ANL/MSD/CP-84938; CONF-951135-29). Argonne, IL: Argonne National Lab. (ANL); 1995.

[2] Xuan Y, Li Q. Heat transfer enhancement of nanofluids. Int J Heat Fluid Flow 2000;21:58-64. [CrossRef]

[3] Buongiorno J. Convective transport in nanofluids. J Heat Transf 2006;128:240-250. [CrossRef]

[4] Koopaee MK, Omidvar A, Jelodari I. Numerical study on the steady-state heat transfer rate of nanofluid filled within square cavity in the presence of oriented magnetic field. Proc Inst Mech Engineer C: J Mech Engineer Sci 2014;228:1348-1362. [CrossRef]

[5] Reddy CS, Kishan N, Shekar BC. MHD boundary layer flow and heat transfer of a nanofluid over a shrinking sheet with mass suction and chemical reaction. J Nanofluids 2015;4:518-527. [CrossRef]

[6] Jelodari I, Nikseresht AH. Effects of Lorentz force and induced electrical field on the thermal performance of a magnetic nanofluid-filled cubic cavity. J Molecular Liquids 2018;252:296-310. [CrossRef]

[7] Kilic M, Ali HM. Numerical investigation of combined effect of nanofluids and multiple impinging jets on heat transfer. Therm Sci 2019;23:3165-3173. [CrossRef]

[8] Shah Z, Sheikholeslami M, Kumam P, Shutaywi M, Thounthong P. CFD simulation of water-based hybrid nanofluid inside a porous enclosure employing Lorentz forces. IEEE Access 2019;7:177177-177186. [CrossRef]

[9] Ahmad M, Muhammad T, Ahmad I, Aly S. Time-dependent 3D flow of viscoelastic nanofluid over an unsteady stretching surface. Physica A Stat Mech Appl 2020;551:124004. [CrossRef]
[10] Acharya N. On the flow patterns and thermal behaviour of hybrid nanofluid flow inside a micro-channel in presence of radiative solar energy. J Therm Anal Calorim 2020;141:1425-1442. [CrossRef]
[11] Dogonchi AS, Sadeghi MS, Ghodrat M, Chamkha AJ, Elmasry Y, Alsulami R. Natural convection and entropy generation of a nanoliquid in a crown wavy cavity: Effect of thermo-physical parameters and cavity shape. Case Stud Therm Engineer 2021;27:101208. [CrossRef]
[12] Waqas H, Bukhari FF, Farooq U, Alqarni MS, Muhammad T. Numerical computation of melting heat transfer in nonlinear radiative flow of hybrid nanofluids due to permeable stretching curved surface. Case Stud Therm Engineer 2021;27:101348. [CrossRef]
[13] Abo-Dahab SM, Abdelhafez MA, Mebarek-Oudina F, Bilal SM. MHD Casson nanofluid flow over nonlinearly heated porous medium in presence of extending surface effect with suction/injection. Indian J Physics 2021;95:2703-2717. [CrossRef]
[14] Swain K, Mahanthesh B. Thermal enhancement of radiating magneto-nanoliquid with nanoparticles aggregation and joule heating: a three-dimensional flow. Arabian J Sci Engineer 2021;46:5865-5873. [CrossRef]
[15] Ho CJ, Cheng CY, Yang TF, Rashidi S, Yan WM. Experimental study on cooling performance of nanofluid flow in a horizontal circular tube. Int J Heat Mass Transf 2021;169:120961. [CrossRef]
[16] Ahmed AM, Zakinyan AR, Wahab WSA. Effect of magnetic field on electroconvection in a thin layer of magnetic nanofluid. Chem Physics Letters 2023;817:140413. [CrossRef]
[17] Selim MM, El-Safty S, Tounsi A, Shenashen M. Review of the impact of the external magnetic field on the characteristics of magnetic nanofluids. Alexandria Engineer J 2023;76:75-89. [CrossRef]
[18] Ullah A, Kilic M, Habib G, Sahin M, Khalid RZ, Sanaullah K. Reliable prediction of thermophysical properties of nanofluids for enhanced heat transfer in process industry: a perspective on bridging the gap between experiments, CFD and machine learning. J Therm Anal Calorim 2023;148:5859-5881. [CrossRef]
[19] Alfvén H. Existence of electromagnetic-hydrodynamic waves. Nature 1942;150:405-406. [CrossRef]
[20] Gundagani M. Finite element solution of thermal radiation effect on unsteady MHD flow past a vertical porous plate with variable suction. Am Acad Scholar Res J 2012;4:3-22. [CrossRef]
[21] Reddy MK, Murali G, Sivaiah S, Babu NVN. Heat and mass transfer effects on unsteady MHD free convection flow past a vertical permeable moving plate with radiation. IJ Appl Math Res 2012;12:189-205. [CrossRef]
[22] Sivaiah S, Murali G, Reddy MCK, Raju RS. Unsteady MHD mixed convection flow past a vertical porous plate in presence of radiation. Int J Basic Appl Sci 2012;1:651-666. [CrossRef]
[23] Gundagani M, Sheri S, Ajit PAUL, Reddy MCK. Radiation effects on an unsteady MHD convective flow past a semi-infinite vertical permeable moving plate embedded in a porous medium with viscous dissipation. Walailak J Sci Tech 2013;10:499-515.
[24] Deepa G, Murali G. Effects of viscous dissipation on unsteady MHD free convective flow with thermophoresis past a radiate inclined permeable plate. Iranian J Sci Tech 2014;38:379-388.
[25] Gupta S, Kumar D, Singh J. Magnetohydrodynamic three-dimensional boundary layer flow and heat transfer of water-driven copper and alumina nanoparticles induced by convective conditions. Int Modern Physics B 2019;33:1950307. [CrossRef]
[26] Umar M, Akhtar R, Sabir Z, Wahab HA, Zhiyu Z, Imran A, et al. Numerical treatment for the three-dimensional Eyring-Powell fluid flow over a stretching sheet with velocity slip and activation energy. Advances in Mathematical Physics 2019:9860471. [CrossRef]
[27] Abdullah Mohamed R, Mahmoud Aly A, Elsayed Ahmed S, Sayed Soliman M. MHD Jeffrey nanofluids flow over a stretching sheet through a porous medium in presence of nonlinear thermal radiation and heat generation/absorption. Chal Nano Micro Scale Sci Tech 2020;8:9-22.
[28] Jabeen K, Mushtaq M, Akram Muntazir RM. Analysis of MHD fluids around a linearly stretching sheet in porous media with thermophoresis, radiation, and chemical reaction. Math Problems Engineer 2020:9685482. [CrossRef]
[29] Anantha Kumar K, Sugunamma V, Sandeep N. Effect of thermal radiation on MHD Casson fluid flow over an exponentially stretching curved sheet. J Therm Anal Calorim 2020;140:2377-2385. [CrossRef]
[30] Goyal R, Vinita, Sharma N, Bhargava R. GFEM analysis of MHD nanofluid flow toward a power-law stretching sheet in the presence of thermodiffusive effect along with regression investigation. Heat Transf 2021;50:234-256. [CrossRef]
[31] Ahmed K, McCash LB, Akbar T, Nadeem S. Effective similarity variables for the computations of MHD flow of Williamson nanofluid over a non-linear stretching surface. Processes 2022;10:1119. [CrossRef]
[32] Mishra P, Kumar D, Kumar J, Abdel-Aty AH, Park C, Yahia IS. Analysis of MHD Williamson micropolar fluid flow in non-Darcian porous media with variable thermal conductivity. Case Stud Therm Engineer 2022;36:102195. [CrossRef]
[33] Casson N. Rheology of Dispersed System. London: Pergamon Press; 1959.

[34] Murali G, Paul AJIT, Babu N. Numerical study of chemical reaction effects on unsteady MHD fluid flow past an infinite vertical plate embedded in a porous medium with variable suction. Electro J Math Anal Appl 2015;3:179-192. [CrossRef]
[35] Bilal S, Malik MY, Hussain A, Khan M. Effects of temperature dependent conductivity and absorptive/generative heat transfer on MHD three dimensional flow of Williamson fluid due to bidirectional non-linear stretching surface. Results Physics 2017;7:204-212. [CrossRef]
[36] Babu N, Murali G, Bhati S. Casson fluid performance on natural convective dissipative Couette flow past an infinite vertically inclined plate filled in porous medium with heat transfer, MHD and hall current effects. Int J Pharmaceut Res 2018;10.
[37] Ganesh Kumar K. Scrutinization of 3D flow and nonlinear radiative heat transfer of non-Newtonian nanoparticles over an exponentially sheet. Int J Numer Methods Heat Fluid Flow 2019;30:2051-2062. [CrossRef]
[38] Ibrahim W, Anbessa T. Three-dimensional MHD mixed convection flow of Casson nanofluid with hall and ion slip effects. Math Problems Engineer 2020:8656147. [CrossRef]
[39] Rao PS, Prakash O, Mishra SR, Sharma RP. Similarity solution of three-dimensional MHD radiative Casson nanofluid motion over a stretching surface with chemical and diffusion-thermo effects. Heat Transf 2020;49:1842-1862. [CrossRef]
[40] Khan MI, Alzahrani F, Hobiny A. Simulation and modeling of second order velocity slip flow of micropolar ferrofluid with Darcy-Forchheimer porous medium. J Mater Res Tech 2020;9:7335-7340. [CrossRef]
[41] Venkata Ramudu AC, Anantha Kumar K, Sugunamma V, Sandeep N. Impact of Soret and Dufour on MHD Casson fluid flow past a stretching surface with convective-diffusive conditions. J Therm Anal Calorim 2022;147:2653-2663. [CrossRef]
[42] Vinita V, Poply V. Impact of outer velocity MHD slip flow and heat transfer of nanofluid past a stretching cylinder. Mater Today Proc 2020;26:3429-3435. [CrossRef]
[43] Renu DEVI, Poply V, Mani MALA. Effect of aligned magnetic field and inclined outer velocity in casson fluid flow over a stretching sheet with heat source. J Therm Engineer 2021;7:823-844. [CrossRef]
[44] Wang Q, Zhao Q. Unsteady aerodynamic characteristics simulations of rotor airfoil under oscillating free stream velocity. Appl Sci 2020;10:1822. [CrossRef]
[45] Irfan M, Farooq MA, Iqra T. Magnetohydrodynamic free stream and heat transfer of nanofluid flow over an exponentially radiating stretching sheet with variable fluid properties. Front Physics 2019;7:186. [CrossRef]
[46] Poply V, Singh P, Yadav AK. Stability analysis of MHD outer velocity flow on a stretching cylinder. Alexandria Engineer J 2018;57:2077-2083. [CrossRef]
[47] Shateyi S. Numerical analysis of three-dimensional MHD nanofluid flow over a stretching sheet with convective boundary conditions through a porous medium. Nanofluid Heat Mass Transf Engineer Problems 2017:65803. [CrossRef]
[48] Khan JA, Mustafa M, Hayat T, Alsaedi A. Three-dimensional flow of nanofluid over a non-linearly stretching sheet: An application to solar energy. Int J Heat Mass Transf 2015;86:158-164. [CrossRef]
[49] Alotaibi H, Althubiti S, Eid MR, Mahny KL. Numerical treatment of MHD flow of Casson nanofluid via convectively heated non-linear extending surface with viscous dissipation and suction/injection effects. Comp Mater Cont 2020;66:229-245. [CrossRef]
[50] Abolbashari MH, Freidoonimehr N, Nazari F, Rashidi MM. Analytical modeling of entropy generation for Casson nano-fluid flow induced by a stretching surface. Adv Powder Tech 2015;26:542-552. [CrossRef]
[51] Reddy Gorla RS, Sidawi I. Free convection on a vertical stretching surface with suction and blowing. Appl Sci Res 1994;52:247-257. [CrossRef]
[52] Wang CY. Free convection on a vertical stretching surface. ZAMM J Appl Math Mech 1989;69:418-420. [CrossRef]